Single-Molecule Charge Transport Modulation Induced by Steric Effects of Side Alkyl Chains

Wenlin Jiang, [†] Zhibing Tan[†], Renad Almughathawi[†], Qingqing Wu,[†] Zitong Liu,* Junyang Liu, Songjun Hou, Guanxin Zhang, Colin J. Lambert,* Wenjing Hong,* Deqing Zhang*

W. Jiang, Prof. Z. Liu, Prof. G. Zhang, Prof. D. Zhang
Beijing National Laboratory for Molecular Sciences, CAS Key Laboratory for Organic Solids, Institute of Chemistry, Chinese Academy of Sciences, Beijing 100190, China.
E-mail: zitong_@iccas.ac.cn, dqzhang@iccas.ac.cn

Z. Tan, J. Liu, Prof. W. Hong
State Key Laboratory of Physical Chemistry of Solid Surfaces, iChEM, College of Chemistry and Chemical Engineering
Xiamen University
Xiamen, Siming South Road (China)
E-mail: whong@xmu.edu.cn

R. Almughathawi, Q. Wu, S. Hou, Prof. C. Lambert
Department of Physics
Lancaster University
Lancaster LA1 4YB (UK)
E-mail: c.lambert@lancaster.ac.uk
[†] These authors contributed equally to this work.

Keywords: single-molecule conductance • side alkyl chain • conjugated molecule • molecular conformation • diketopyrrolopyrrole

Abstract: Experimental investigation of the side chain effects on intramolecular charge transport in π-conjugated molecules is essential, but remains challenging. Herein, the dependence of intra-molecular conductance on the nature of branching alkyl chains is investigated through a combination of the scanning tunneling microscope break junction (STM-BJ) technique and density functional theory. Three thiophene-flanked diketopyrrolopyrrole (DPP) derivatives with different branching alkyl chains (isopentane, 3-methylheptane, and 9-methylnonadecane) are used with phenylthiomethyl groups as the anchoring groups. The results of single-molecule conductance measurements show that as the alkyl chain becomes longer, the torsional angles between the aromatic rings increase due to steric crowding, and therefore, the molecular conductance of DPP decreases due to reduction in conjugation. Both theoretical simulations and ^{1}H NMR spectra demonstrate that the planarity of the DPPs is directly reduced

after introducing longer branching alkyl chains, which leads to the reduced conductance. This work indicates that the effect of insulating side chain on single-molecule conductance cannot be neglected, which should be considered for the design of future organic semiconducting materials.

1. Introduction

The electronic properties of the conjugated molecules play an essential role for organic electronics, which are governed by the electronic structures of the conjugated frameworks and the intermolecular interactions. [1] It is known that the pendant alkyl chains attached to the conjugated backbone not only improve the solubility, but also influence the intermolecular/inter-chain orderly packing, [2] and may also lead to the changes of electronic structure of the conjugated backbone. [3] However, it remains challenging to distinguish the contribution of the side-chain on the intramolecular charge transport and the intermolecular packing. For that, the charge transport through the single-molecule diketopyrrolopyrrole (DPP) junctions[4] provides a unique opportunity to study the role of the side-chain on the intramolecular charge transport from the single-molecule level.

In the charge transport investigations through the single-molecule junctions, the conjugated molecules typically possess alkyl chains as soluble groups attached to the periphery of conjugated cores to have solubility for the processing and characterization. [4-6] In some cases, studies suggested that the side-chains attached to the rigid oligo-phenylene-ethynylene (OPE) building blocks lead to no significant changes in the electronic structure of the conjugated backbone, and thus alkyl chains are replaced by methyl groups in most of the combined theoretical investigations. [6] However, the role of the side-chains on the conformation control of the conjugated frameworks remained unexplored. Our previous studies had suggested that the backbone planarity and rigidity were improved when we replaced one bulky branching alkyl chain in the diketopyrrolopyrrole (DPP)-based polymers with one linear alkyl chain in each

DPP unit. [3a] Thus the experimental investigations of DPP-based conjugated molecules may offer new insight into the side chain effects on intramolecular charge transport in π-conjugated molecules.

In this paper, we report single-molecule conductance studies of three diketopyrrolopyrrole (DPP)-based conjugated molecules **DPP-1/4**, **DPP-2/6**, and **DPP-8/12** with the STM-BJ technique, and investigate the side chain effects on their intramolecular charge transport (**Scheme 1**). Compounds **DPP-1/4**, **DPP-2/6**, and **DPP-8/12** possess the same conjugated skeleton and the same anchoring groups (-SCH_3), but they bear different side alkyl chains, with isopentane (1/4), 3-methylheptane (2/6) and 9-methylnonadecane (8/12) linked to the DPP units in **DPP-1/4**, **DPP-2/6**, and **DPP-8/12**, respectively. It is noted that these alkyl chains are widely utilized in the construction of DPP-based organic and polymeric semiconductors. [7] The results reveal that the single-molecule conductance of **DPP-1/4**, **DPP-2/6**, and **DPP-8/12** decreases in the following order: **DPP-1/4** > **DPP-2/6** > **DPP-8/12**, by increasing the length and bulkiness of alkyl chains. Theoretical studies in combination with ^{1}H NMR data reveal that the effect of pendant alkyl chains on the conjugated backbone conformation (and planarity), and thus the single-molecule conductance of **DPP-1/4**, **DPP-2/6**, and **DPP-8/12** cannot be neglected. The calculations show that the torsional angles among the conjugated units of **DPP-1/4**, **DPP-2/6**, and **DPP-8/12**, and the respective transmission spectra are varied by changing the side alkyl chains, which correlates with the single-molecule conductance studies. Therefore, the insulating side alkyl chains can be used to manipulate the single-molecule conductance, offering potential applications in single molecular electronic devices.

Scheme 1.

2. Results and Discussion

2.1. Single-molecule conductance measurements and the dependence on the length of alkyl chains

The three DPP molecules, **DPP-1/4**, **DPP-2/6**, and **DPP-8/12** (**Scheme 1**), were synthesized and their structures were characterized with NMR and MS spectra as well as elemental analysis (see Supporting Information). The two phenylthiomethyl groups in **DPP-1/4**, **DPP-2/6**, and **DPP-8/12** were used as the anchoring groups to connect the respective molecules with the gold electrodes to form single-molecule junctions.

A homemade STM-BJ setup[8] was used to measure the single-molecule conductance of **DPP-1/4**, **DPP-2/6**, and **DPP-8/12,** which were separately dissolved in mesitylene (TMB) to reach a concentration of 0.1 mM. As shown in Figure S1, typically, the solution is dripped onto a silicon wafer on which gold is evaporated. During the measurement, a gold tip adhered to the piezo was controlled to immerse into the solution and contact with the substrate. The optimized control system can control the tip repeatedly contacting and leaving the substrate (see Supporting Information for more details). When the two electrodes split, a nanogap matched with the length of the target molecule is formed, and as a consequence, the molecule can be connected with the electrodes through the anchoring groups (**Scheme 1**). A 100 mV bias was applied between the tip and the substrate, and the current through the two electrodes was monitored in real-time. The conductance-displacement curves were recorded and shown in **Figure 1a**. It can be seen that an obvious plateau appears ranging from 10^{-3} G_0 to 10^{-5} G_0 for **DPP-1/4**, **DPP-2/6**, and **DPP-8/12**, while the conductance decreases exponentially with the increased displacement and the curves are smooth when the pure solvent (mesitylene) was measured under the same condition. The data show that i) the molecule was assembled on the gold electrode to form the molecular junction, and ii) the measured conductance was attributed to the formation of molecular junction during the measurements.

Figure 1

2D conductance histograms were acquired by superimposing such ~1000 conductance traces. As shown in **Figure 1b** and Figure S2, the 2D conductance histograms of **DPP-1/4**, **DPP-2/6**

and **DPP-8/12** display the distinguished conductance intensity cloud, but such conductance intensity cloud is not observable for the blank experiment (Figure S3). Moreover, the relative displacement distribution (see the inset of **Figure 1b**) shows that the maximum probability distribution of conductance appears at the displacement of ~1.5 nm, which is close to the sum of the molecular length (along the conduction path) of **DPP-1/4** or **DPP-2/6** or **DPP-8/12** plus the Au relaxation gap (~0.5 nm[4c,9]). To obtain the molecular conductance, we constructed 1D conductance histograms as shown in **Figure 1c**. The sharp peak at G_0 indicates the formation of point contact between gold and gold atoms (G_0 is quantum conductance and is equal to $2e^2/h$). The most probable conductance values were determined from the results of the Gauss fitting of conductance peak. The molecular conductances of **DPP-1/4**, **DPP-2/6** and **DPP-8/12** are estimated to be $10^{-3.55}$ G_0, $10^{-3.96}$ G_0, and $10^{-4.33}$ G_0 respectively. The short, high-conductance peak of **DPP 8/12** in **Figure 1c** may be caused by metal (Au)–π coupling. [10]

The results reveal that the molecular conductances of **DPP-1/4**, **DPP-2/6** and **DPP-8/12** are dependent on the structures of the side alkyl chains; the molecular conductance decreases gradually by increasing the lengths of alkyl chains as shown in **Figure 1d**.

2.2. Mechanism studies

DPP-1/4, **DPP-2/6** and **DPP-8/12** bear the same conjugated units and anchoring groups, but they possess different alkyl chains. The fact that **DPP-1/4**, **DPP-2/6** and **DPP-8/12** show different molecular conductances can be attributed to their different conformations of conjugated backbones in terms of dihedral angles between the conjugated units. We assume that the different alkyl chains in **DPP-1/4**, **DPP-2/6** and **DPP-8/12** may affect the conformations of the conjugated backbones. Theoretical calculations were carried out at the level of density functional theory (DFT, see Supporting Information) in order to understand the effect of side alkyl chains on molecular conductance. We first obtained the fully optimized gas-phase molecules and then built the junctions with molecules attached to two pyramidal-shaped

electrodes via SMe anchor groups. After the re-optimization of junctions, the mean-field Hamiltonian of each molecular geometry was obtained, and then combined with quantum transport theory[11] to calculate the transmission coefficients T (*E*).

With **DPP-8/12** as an example, the theoretical calculations afforded two stable conformers *A* and *B* (in which the intramolecular S---O interactions are observable, see **Figure 2a**) in terms of the positions of the side alkyl chains relative to the conjugated backbone. Between the two conformers, which show different dihedral angles between the conjugated units, conformer *B* is most stable. In conformer *B*, the dihedral angles between the central DPP core and the left flanking thiophene is 37.3°, and that between the central DPP core and the right flanking thiophene is 23.1°. It is obvious that the conjugated backbone of **DPP-8/12** is twisted. Similarly, theoretical calculations were performed for **DPP-1/4** and **DPP-2/6**, and for comparison, the calculation was also extended to **DPP-CH_3** in which the alkyl chains are replaced by $–CH_3$ groups. **Table 1** lists the dihedral angles between the central DPP core and the left/right flanking thiophenes. For **DPP-1/4** and **DPP-CH_3** in which the alkyl chains are short, the conjugated units are almost coplanar. By elongating the alkyl chains as in **DPP-2/6** and **DPP-8/12** the dihedral angles become large and thus the conjugated backbones are nonplanar.

Figure 2

Table 1

From the respective transmission coefficients, conformer *A* of **DPP-8/12**, which is more planar than conformer *B*, is predicted to possess a higher molecular conductance than conformer *B* (Figure S4). Moreover, further calculations were performed with conformer *B* in which the two branching alkyl chains were replaced by two methyl groups and the dihedral angles between the central DPP core and flanking thiophenes were manually changed as shown in

Figure 2b-2c. The results show that the molecular conductance decreased gradually by increasing the dihedral angles. The Fermi energy of the system is difficult to be predicted due to the complicated experimental environment, such as the shape of the electrodes and the effect of solvents. However, it is believed that the Fermi energy is located somewhere in the HOMO-LUMO gap. The transmission functions in the whole HOMO-LUMO gap show a decreasing trend. The relationship between the transmission function around middle point of HOMO-LUMO gap and the torsion angle θ follows approximately $T(E, \theta) \propto \cos^6 \theta$ which is not the expected $\cos^8 \theta$ due to several other effects present in the system, e.g. the electrostatic effects between S of thiophene, O of DPP core and H of phenyl ring. [12] (see more details in Figure S9) Therefore, it is expected that **DPP-1/4**, **DPP-2/6** and **DPP-8/12** show different molecular conductances because of the different conformations of their conjugated backbones. Based on their most stable conformers, the respective transmission coefficients were calculated for **DPP-1/4**, **DPP-2/6** and **DPP-8/12** as well as **DPP-CH$_3$**. The calculation results were shown in **Figure 3**, the molecular conductances of **DPP-CH$_3$**, **DPP-1/4**, **DPP-2/6** and **DPP-8/12** increase in the following order: **DPP-8/12** < **DPP-2/6** < **DPP-1/4** < **DPP-CH$_3$**. The calculations agree well with the molecular conductances measured experimentally as mentioned above. In short, as the lengths of side alkyl chains increase, the conjugated backbones become nonplanar with enlarging the dihedral angles, leading to the dropping of molecular conductance.

Figure 3

Alternatively, **DPP-8/12** can also adopt stable conformers such as *A*' and *B*' (Figure S5) in which short interatomic contact exists between the oxygen atoms of the central DPP core and the hydrogen atoms of the flanking thiophenes. [13] Conformer *B*' in which the alkyl chains are close to the conjugated backbone is more stable in energy than *A*', but its backbone becomes more twisted. In comparison, the optimized geometry of the analogue molecule in which the alkyl chains are replaced by the methyl groups is more planar. Further calculations of

transmission coefficients show that conformer *B*' has a low molecular conductance (Figure S6). Subsequently, we performed calculations by keeping the backbone conformation of *B*' and substituting the long alkyl chains with -CH_3 groups. It is clear when the long alkyl chains are removed, while retaining the same conformation, the electrical conductance does not change (red and yellow curves in Figure S7), which reveals that the alkyl chains make no direct contribution to molecular conductance.

These calculations show i) the conformation of conjugated backbones of these DPP molecules is affected by the structures of side alkyl chains, and the dihedral angles among the conjugated units are enlarged by elongating the alkyl chains, and ii) consequently the effect of alkyl chains on the molecular conductance cannot be neglected for these DPP molecules and the molecular conductance becomes low by increasing the lengths of side alkyl chains. Mayor and their coworkers previously reported single-molecule junction towards biphenyl systems with controlled torsion angles.[14] But, the alkyl chains were used as the bridging chains to connect biphenyl molecules at 2,2'-positions, which are different from the side alkyl chains discussed in this paper.

In fact, the effect of the side alkyl chains on the conformation of conjugated backbone is also supported by the ^{1}H NMR spectra of **DPP-1/4**, **DPP-2/6** and **DPP-8/12**, which were measured under the same condition. As shown in **Figure 4**, the chemical shift for the α-protons of the thiophenes is up-field shifted slightly from 8.99 ppm (**DPP-1/4**) to 8.93 ppm (**DPP-2/6**) and 8.90 ppm (**DPP-8/12**), indicating that the conjugation degree is reduced when introducing longer branching alkyl chains. Moreover, the chemical shift and coupling pattern for β-protons of the thiophenes are also slightly varied. In comparison with **DPP-1/4**, **DPP-2/6** and **DPP-8/12** possess larger torsional angles, namely, the DPP unit and the flanked thiophenes become non-planar for **DPP-2/6** and **DPP-8/12**, the intramolecular charge transfer from thiophenes to DPP units will be weaker by comparing with **DPP-1/4**; as a consequence, the electron densities

around α-protons and β-protons will be higher, leading to up-field shifts. The calculated torsional angles increase in the following order: **DPP-1/4** < **DPP-2/6** < **DPP-8/12**. This agrees well with the up-field shifts for α-protons and β-protons of **DPP-2/6** and **DPP-8/12** in comparison with those of **DPP-1/4** (see **Figure 4**). We also measured the low-temperature ^{1}H NMR spectra at 233K (**Figure S10**). Although the peak became sharp at 233K, the α-proton chemical shifts of three DPP compounds still followed the rule as we found above. Thus, these ^{1}H NMR data agree well with the theoretical prediction that the conformation of conjugated backbones of **DPP-1/4**, **DPP-2/6** and **DPP-8/12** are affected by the lengths of side alkyl chains.

Figure 4

3. Conclusion

In this paper, we investigated the changes in intra-molecular conductance induced by varying the branching alkyl chains through a combination of the STM-BJ technique and DFT simulations. Three thiophene-flanked DPP derivatives with different branching alkyl chains of isopentane, 3-methylheptane, and 9-methylnonadecane were used, and phenylthiomethyl groups were used as anchors. The STM-BJ results show that as the alkyl chain becomes larger, the resulting molecular conductance is decreased. Both theoretical simulations and ^{1}H NMR spectra demonstrate that the planarity of the DPPs is directly reduced after introducing longer branching alkyl chains, causing reduced conductance. This work demonstrates that insulating side chains' effect on single-molecule conductance cannot be neglected, and should be considered for the design of future organic semiconducting materials.

Supporting Information
Supporting Information is available from the Wiley Online Library or from the author.

Acknowledgements
We thank the financial support of the National Key R&D Program of China (2018YFE0200700, 2017YFA0204701, 2017YFA0204902), NSFC (21661132006, 61890943, 21790360, 21722305, 21933012, 21673195), the Beijing National Laboratory for Molecular Sciences

(BNLMS202005). Colin J. Lambert acknowledges financial support from the UK EPSRC, through grant nos. EP/M014452/1, EP/P027156/1 and EP/N03337X/1. This work is supported by the European Commission through the FET Open project 767187–QuIET.

Received: ((will be filled in by the editorial staff))
Revised: ((will be filled in by the editorial staff))
Published online: ((will be filled in by the editorial staff))

References

[1] a) V. Coropceanu, J. Cornil, D. A. da Silva Filho, Y. Olivier, R. Silbey, J. L. Bredas, *Chem. Rev.* **2007**, *107*, 926-952; b) Z. Shuai, H. Geng, W. Xu, Y. Liao, J. M. Andre, *Chem. Soc. Rev.* **2014**, *43*, 2662-2679; c) R. Noriega, J. Rivnay, K. Vandewal, F. P. Koch, N. Stingelin, P. Smith, M. F. Toney, A. Salleo, *Nat. Mater.* **2013**, *12*, 1038-1044.

[2] a) Y. Yang, Z. Liu, G. Zhang, X. Zhang, D. Zhang, *Adv. Mater.* **2019**, *31*, e1903104; b) T. Lei, J.-Y. Wang, J. Pei, *Chem. Mater.* **2013**, *26*, 594-603; c) J. Mei, Z. Bao, *Chem. Mater.* **2013**, 26, 604-615; d) Z. Liu, G. Zhang, D. Zhang, *Acc. Chem. Res.* **2018**, *51*, 1422-1432; e) P. Zhan, W. Zhang, I. E. Jacobs, D. M. Nisson, R. Xie, A. R. Weissen, R. H. Colby, A. J. Moulé, S. T. Milner, J. K. Maranas, E. D. Gomez, *J. Polym. Sci., Part B: Polym. Phys*. **2018**, *56*, 1193-1202.

[3] a) Z. Wang, Z. Liu, L. Ning, M. Xiao, Y. Yi, Z. Cai, A. Sadhanala, G. Zhang, W. Chen, H. Sirringhaus, D. Zhang, *Chem. Mater*. **2018**, *30*, 3090-3100; b) J. Tian, L. Fu, Z. Liu, H. Geng, Y. Sun, G. Lin, X. Zhang, G. Zhang, D. Zhang, *Adv. Funct. Mater.* **2019**, *29*, 1807176.

[4] a) Y. -P. Zhang, L. -C. Chen, Z. -Q. Zhang, J. -J. Cao, C. Tang, J. Liu, L. -L. Duan, Y. Huo, X. Shao, W. Hong, H. -L. Zhang, *J. Am. Chem. Soc.* **2018**, *140*, 6531-6535; b) Y. Zang, S. Ray, E. D. Fung, A. Borges, M. H. Garner, M. L. Steigerwald, G. C. Solomon, S. Patil, L. Venkataraman, *J. Am. Chem. Soc.* **2018**, *140*, 13167-13170; c) Y. Zang, E. D. Fung, T. Fu, S. Ray, M. H. Garner, A. Borges, M. L. Steigerwald, S. Patil, G. Solomon, L. Venkataraman, *Nano. Lett.* **2021**, *21*, 673-679; d) Z. Tan, W. Jiang, C. Tang, L.-C. Chen, L. Chen, J. Liu, Z. Liu, H.-L. Zhang, D. Zhang, W. Hong, *CCS Chemistry* **2021**, 929-937.

[5] a) X. Guo, D. Xiang, Y. Li, Molecular-Scale Electronics: Concept, Fabrication and Applications, Book, Wiley-VCH, **2020**, ISBN:978-3-527-34548-9; b) N. Xin, X. Kong, Y. P. Zhang, C. Jia, L. Liu, Y. Gong, W. Zhang, S. Wang, G. Zhang, H. L. Zhang, H. Guo, X. Guo, *Adv. Electron. Mater.* **2020**, *6*, 1901237; c) Z. Cai, W. Y. Lo, T. Zheng, L. Li, N. Zhang, Y. Hu, L. Yu, *J. Am. Chem. Soc*. **2016**, *138*, 10630-10635; d) Z. Cai, N. Zhang, M. A. Awais, A. S. Filatov, L. Yu, *Angew. Chem. Int. Ed*. **2018**, *57*, 6442-6448; e) L. Venkataraman, J. E. Klare, C. Nuckolls, M. S. Hybertsen, M. L. Steigerwald, *Nature* **2006**, *442*, 904-907; f) A. Mishchenko, L. A. Zotti, D. Vonlanthen, M. Burkle, F. Pauly, J. C. Cuevas, M. Mayor, T. Wandlowski, *J. Am. Chem. Soc.* **2011**, *133*, 184-187; g) S. Soni, G. Ye, J. Zheng, Y. Zhang, A. Asyuda, M. Zharnikov, W. Hong, R. C. Chiechi, *Angew. Chem. Int. Ed.* **2020**, *59*, 14308-14312; h) M. Carlotti, A. Kovalchuk, T. Wachter, X. Qiu, M. Zharnikov, R. C. Chiechi, *Nat. Commun.* **2016**, *7*, 13904; i) D. Kos, G. Di Martino, A. Boehmke, B. de Nijs, D. Berta, T. Foldes, S. Sangtarash, E. Rosta, H. Sadeghi, J. J. Baumberg, *Nat. Commun.* **2020**, *11*, 5905; j) Y. Zang, T. Fu, Q. Zou, F. Ng, H. Li, M. L. Steigerwald, C. Nuckolls, L. Venkataraman, *Nano. Lett.* **2020**, *20*, 8415-8419.

[6] a) S. Martin, I. Grace, M. R. Bryce, C. Wang, R. Jitchati, A. S. Batsanov, S. J. Higgins, C. J. Lambert, R. J. Nichols, *J. Am. Chem. Soc.* **2010**, *132*, 9157-9164; b) R. Frisenda, V. A. Janssen, F. C. Grozema, H. S. van der Zant, N. Renaud, *Nat. Chem.* **2016**, *8*, 1099-1104.

[7] a) Q. Liu, S. E. Bottle, P. Sonar, *Adv. Mater.* **2020**, *32*, e1903882; b) M. Grzybowski, D. T. Gryko, *Adv. Opt. Mater.* **2015**, *3*, 280-320; c) Z. Yi, S. Wang, Y. Liu, *Adv. Mater.* **2015**, *27*, 3589-3606; d) C. B. Nielsen, M. Turbiez, I. McCulloch, *Adv. Mater.* **2013**, *25*, 1859-1880; e) N. Luo, G. Zhang, Z. Liu, *Organ. Chem. Front.* **2021**, DOI:10.1039/D1QO00613D.

[8] a) L. Wang, Z. L. Gong, S. Y. Li, W. Hong, Y. W. Zhong, D. Wang, L. J. Wan, *Angew. Chem. Int. Ed.* **2016**, *55*, 12393-12397; b) C. Tang, L. Chen, L. Zhang, Z. Chen, G. Li, Z. Yan, L. Lin, J. Liu, L. Huang, Y. Ye, Y. Hua, J. Shi, H. Xia, W. Hong, *Angew. Chem. Int.*

Ed. **2019**, *58*, 10601-10605; c) L. Chen, Y. -H. Wang, B. He, H. Nie, R. Hu, F. Huang, A. Qin, X. -S. Zhou, Z. Zhao, B. Z. Tang, *Angew. Chem. Int. Ed.* **2015**, *54*, 4231-4235.

[9] W. Hong, D. Z. Manrique, P. Moreno-Garcia, M. Gulcur, A. Mishchenko, C. J. Lambert, M. R. Bryce, T. Wandlowski, *J. Am. Chem. Soc.* **2012**, *134*, 2292-2304.

[10] J. S. Meisner, S. Ahn, S. V. Aradhya, M. Krikorian, R. Parameswaran, M. Steigerwald, L. Venkataraman, C. Nuckolls, *J. Am. Chem. Soc.* **2012**, *134*, 20440-20445.

[11] J. Ferrer, C. J. Lambert, V. M. García-Suárez, D. Z. Manrique, D. Visontai, L. Oroszlany, R. Rodríguez-Ferradás, I. Grace, S. W. D. Bailey, K. Gillemot, H. Sadeghi, L. A. Algharagholy, *New J. Phys.* **2014**, *16*, 093029.

[12] a) Finch, C. M.; Sirichantaropass, S.; Bailey, S. W.; Grace, I. M.; García-Suárez, V. M.; Lambert, C. J. Conformation Dependence of Molecular Conductance: Chemistry versus Geometry. *J. Phys. Condens. Matter* **2008**, 20, 022203; b) Wu, Q.; Hou, S.; Sadeghi, H.; Lambert, C. A Single-Molecule Porphyrin-Based Switch for Graphene Nano-Gaps. *Nanoscale* **2018**, 10, 6524–6530.

[13] a) M. A. Naik, N. Venkatramaiah, C. Kanimozhi, S. Patil, *J. Phys. Chem. C* **2012**, *116*, 26128-26137; b) C. Fu, F. Bélanger-Gariépy, D. F. Perepichka, *CrystEngComm* **2016**, *18*, 4285-4289; c) Y. Qiao, Y. Guo, C. Yu, F. Zhang, W. Xu, Y. Liu, D. Zhu, *J. Am. Chem. Soc.* **2012**, *134*, 4084-4087.

[14] D. Vonlanthen, A. Mishchenko, M. Elbing, M. Neuburger, T. Wandlowski, M. Mayor, *Angew. Chem. Int. Ed.* **2009**, *48*, 8886-8890.

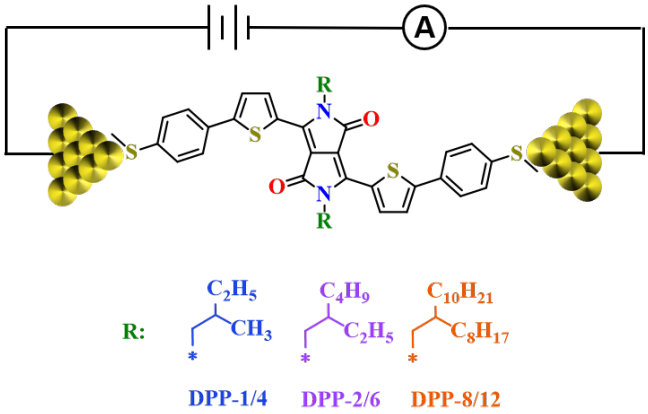

Scheme 1. Schematic of DPP junction and chemical structures of **DPP-1/4**, **DPP-2/6**, and **DPP-8/12** with different side alkyl chains.

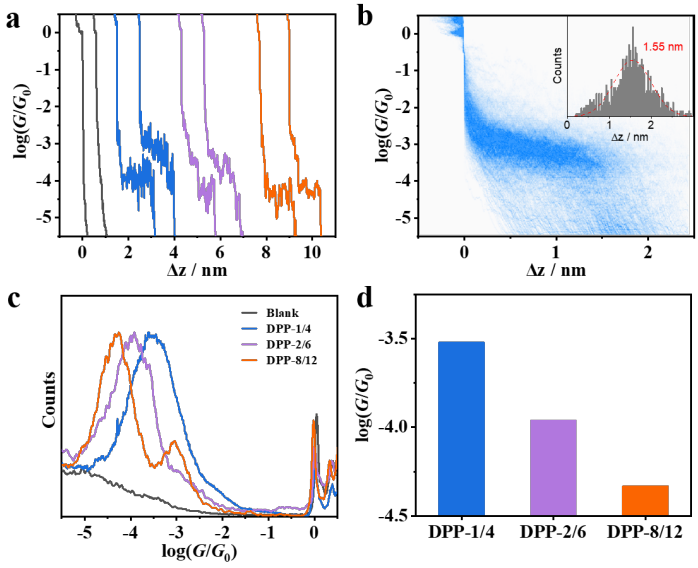

Figure 1. a) Typical individual conductance-displacement curves for **DPP-1/4** (*blue*), **DPP-2/6** (*purple*) and **DPP-8/12** (*orange*). The light grey curves represent blank experiments; b) 2D conductance histogram of DPP-1/4 obtained from ~1000 traces; Inset: the relative displacement distribution; c) 1D conductance histograms of blank (*light grey*), **DPP-1/4** (*blue*), **DPP-2/6** (*purple*), and **DPP-8/12** (*orange*). d) The comparison of the conductance of **DPP-1/4** (*blue*), **DPP-2/6** (*purple*) and **DPP-8/12** (*orange*).

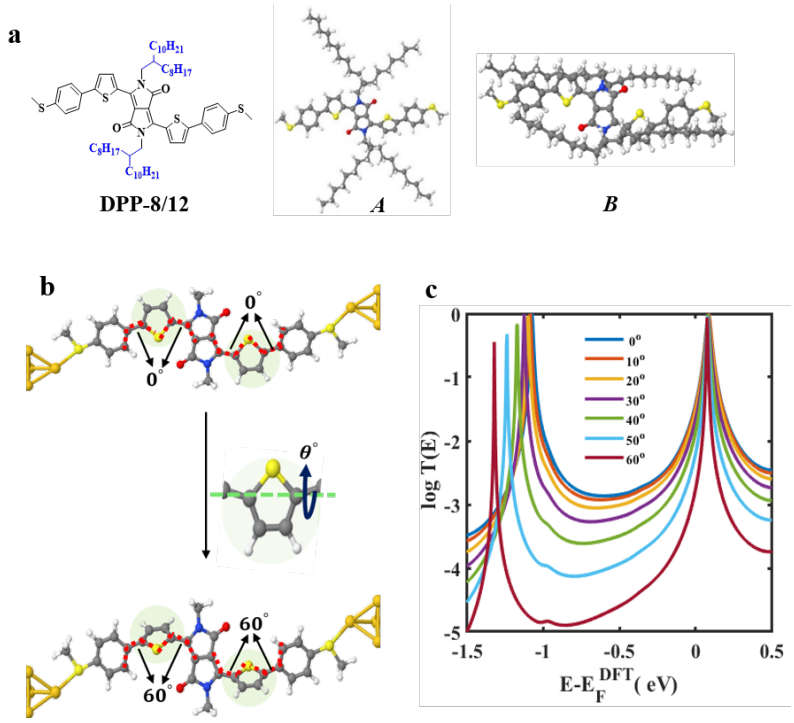

Figure 2. a) Conformations of **DPP-8/12** (S---O) in terms of the positions of the alkyl side chains relative to the backbone. Conformer *A* expanded into the nearby space. The dihedral angle between the left thiophene and DPP-core is 25° and between the right thiophene and the core is 18°. *B* is more compact and more energetically stable compared to conformer *A* by 0.62 eV. In this case, the dihedral angles between the left and right thiophenes and the DPP-backbone are 37.3° and 23.1° respectively. b) Junction formation of the thiophene-DPP core connected to the gold via -SMe with various torsional angles from 0° to 60° between the two planes of left/right flanking thiophene and the rest part of molecule (See **Figure S8** of SI). c) The corresponding transmission functions for molecule DPP-CH_3 displayed in b). The blue curve stands for transmission function of the coplanar conformation (0° dihedral angle, top panel of 2b), while the other colored curves represent those of the conformations with torsional angles up to angle 60° (bottom panel of 2b, see more details in **Figure S8** of SI).

Table 1. The calculated dihedral angles of DPP and flanked thiophenes caused by the presence of alkyl side chains.

Compounds	**Torsional angle (°)**	
	Left flanking thiophene/DPP	Right flanking thiophene/DPP
DPP-1/4	0.5	4.2
DPP-2/6	19.7	32.9
DPP-8/12	37.3	23.1
DPP-CH_3	3.2	1.1

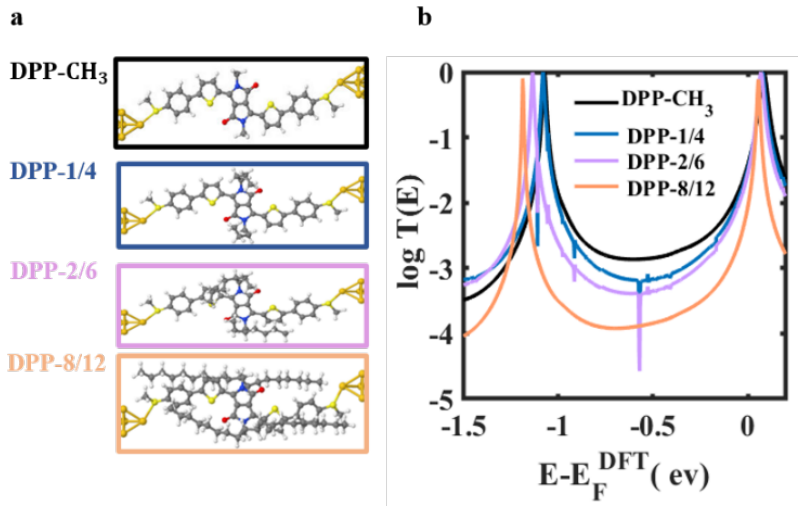

Figure 3. DFT-based transmission functions for DPPs (S---O) with three different alkyl side chains. a) Optimised junction of the single molecules named as **DPP-CH$_3$**, **DPP-1/4**, **DPP-2/6** and **DPP-8/12**, respectively. b) Corresponding transmission coefficients against Fermi energy E_F.

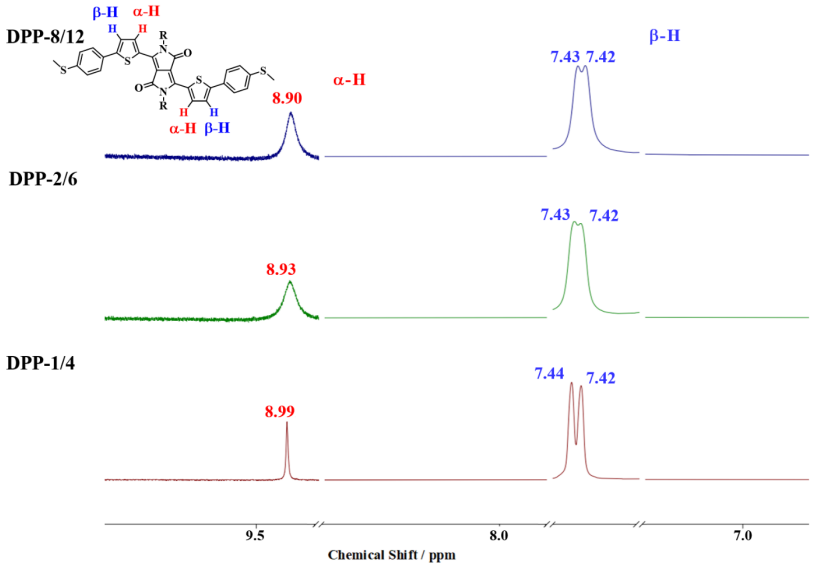

Figure 4. ^{1}H NMR spectra (400 MHz, 298 K) for **DPP-1/4**, **DPP-2/6**, and **DPP-8/12** in $CDCl_3$; the concentration of each sample was 5×10^{-4} M.

Table of contents

The intra-molecular conductance variations by varying the branching alkyl chains were investigated through STM-BJ technique. Both theoretical simulations and ^{1}H NMR spectra demonstrate that the planarity of the conjugated molecule is directly reduced after introducing longer branching alkyl chains, causing reduced conductance. This work provides a way to control the single-molecule conductance, which should be considered for future organic semiconducting material design.

Wenlin Jiang,[†] Zhibing Tan[†], Renad Almughathawi[†], Qingqing Wu,[†] Zitong Liu,* Junyang Liu, Songjun Hou, Guanxin Zhang, Colin J. Lambert,* Wenjing Hong,* Deqing Zhang*

Single-Molecule Charge Transport Modulation Induced by Side Alkyl Chains

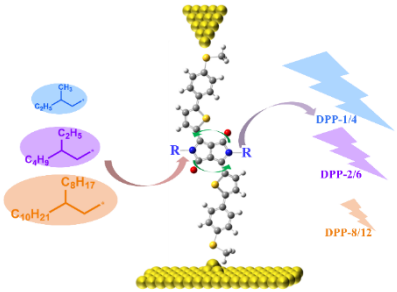

Supporting Information

Single-Molecule Charge Transport Modulation Induced by Steric Effects of Side Alkyl Chains

Wenlin Jiang, [†] Zhibing Tan[†], Renad Almughathawi[†], Qingqing Wu,[†] Zitong Liu,* Junyang Liu, Songjun Hou, Guanxin Zhang, Colin J. Lambert,* Wenjing Hong,* Deqing Zhang*

W. Jiang, Prof. Z. Liu, Prof. G. Zhang, Prof. D. Zhang
Beijing National Laboratory for Molecular Sciences, CAS Key Laboratory for Organic Solids, Institute of Chemistry, Chinese Academy of Sciences, Beijing 100190, China.
E-mail: zitong_@iccas.ac.cn, dqzhang@iccas.ac.cn
Z. Tan, J. Liu, Prof. W. Hong
State Key Laboratory of Physical Chemistry of Solid Surfaces, iChEM, College of Chemistry and Chemical Engineering
Xiamen University
Xiamen, Siming South Road (China)
E-mail: whong@xmu.edu.cn
R. Almughathawi, Q. Wu, S. Hou, Prof. C. Lambert
Department of Physics
Lancaster University
Lancaster LA1 4YB (UK)
E-mail: c.lambert@lancaster.ac.uk
[†] These authors contributed equally to this work.

Keywords: single-molecule conductance • side alkyl chain • conjugated molecule • molecular conformation • diketopyrrolopyrrole

Table of Contents

1. Synthesis

1.1 Materials and characterization techniques

The reagents and starting materials including compounds **M1** and **M3** were commercially available and used without any further purification, if not specified elsewhere. Compounds **M4** and **M5** were synthesized according to the previous reports.[S1-S3] ^{1}H and ^{13}C NMR spectra were recorded on Bruker AVANCE III 400 MHz and 500 MHz spectrometers. Mass spectra were

determined with a Bruker Solarix-XR high-resolution mass spectrometer. Elemental analysis was conducted on a Carlo-Erba-1106 instrument.

1.2 Synthetic experiments

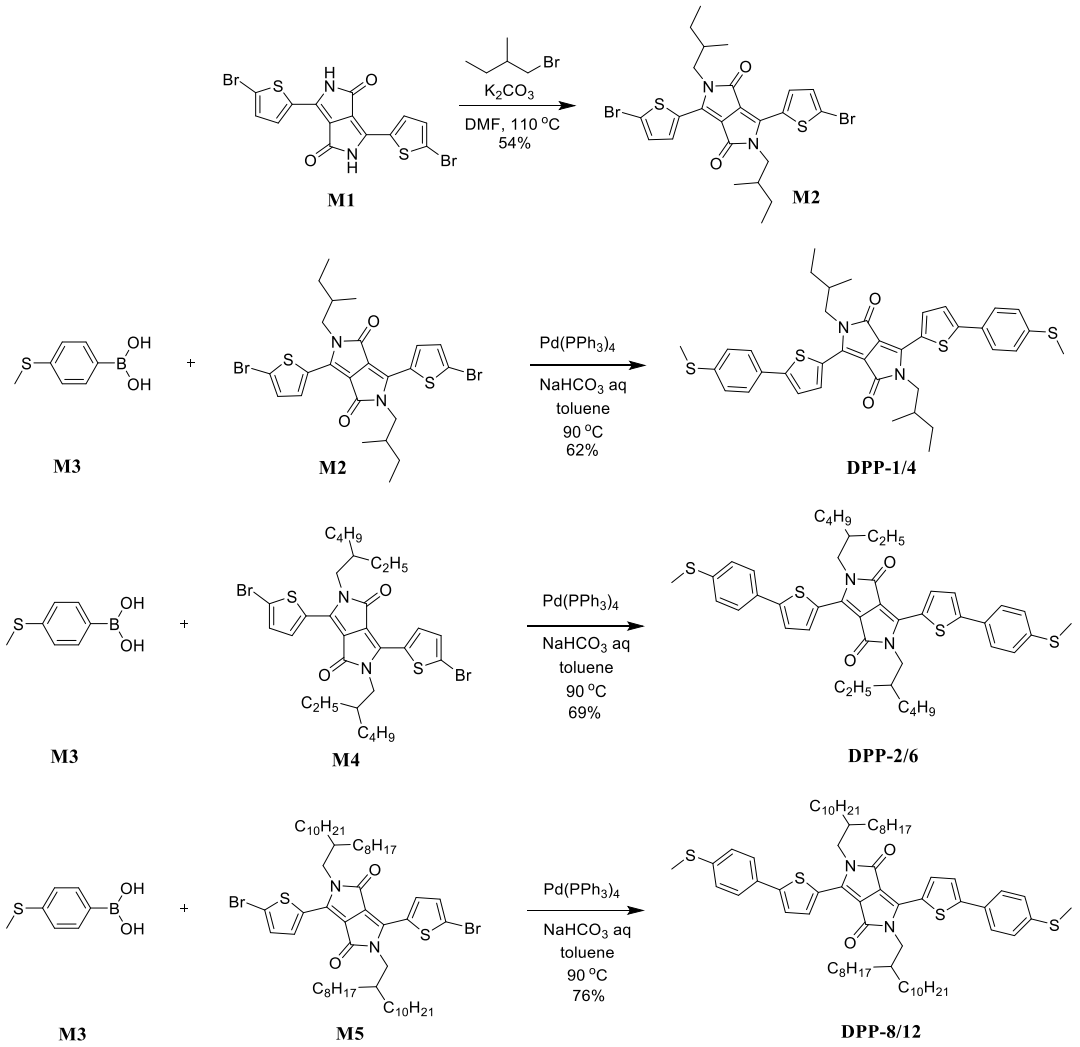

Scheme S1. Synthetic routes to **DPP-1/4**, **DPP-2/6**, and **DPP-8/12**.

Synthesis of **M2**

Compound **M1** (4.0 g, 8.73 mmol) and K_2CO_3 (4.8 g, 34.78 mmol) were added to a 250 mL double-neck round-bottom flask, and 150 mL of dry DMF was injected by syringe under a nitrogen atmosphere. The reaction was heated to 110 °C for 30 min. 1-bromo-2-methylbutane (6.6 g, 43.65 mmol) was added, and the reaction mixture was stirred for 8 h at 110 °C. Solvents were removed by rotary evaporation and the residue was purified by column chromatography with CH_2Cl_2 and petroleum ether (60-90 °C) (1:2, *v/v*) as the eluent. **M2** was obtained as a red-purple solid (2.82 g, 54%). ^{1}H NMR ($CDCl_3$, 400 MHz): δ 8.71 (d, *J* = 4.0 Hz, 2H), 7.23 (d, *J* = 4.0 Hz, 2H), 3.94 – 3.82 (m, 4H), 1.93 – 1.85 (m, 2H), 1.53 – 1.43 (m, 2H), 1.28 – 1.16 (m, 2H), 0.94 – 0.90 (m, 12H). ^{13}C NMR ($CDCl_3$, 100 MHz): δ 161.4, 139.3, 135.6, 131.5, 131.2, 119.1, 107.9, 47.7, 35.4, 26.9, 16.6, 11.2. HR-MS (MALDI-TOF): calcd. for

$C_{24}H_{26}Br_2N_2O_2S_2$ (M^+) 595.9802; Found: 595.9801. Anal. Calcd. for $C_{24}H_{26}Br_2N_2O_2S_2$: C, 48.17; H, 4.38; N, 4.68; S, 10.72; Found: C, 48.11; H, 4.38; N, 4.67; S, 10.86.

Synthesis of **DPP-1/4**

To a Schlenk flask equipped with a stir bar was added compound **M2** (100 mg, 0.167 mmol), compound **M3** (79 mg, 0.47 mmol), $Pd(PPh_3)_4$ (9.7 mg, 8.39 μmol). The vessel was sealed and evacuated/backfilled with nitrogen for three times, followed by the addition of toluene (20 mL) and a degassed 2.0 mL of saturated aqueous solution of $NaHCO_3$ via syringe. The mixture was heated at 90 °C for 8 h. After cooling, the mixture was directly evaporated to remove the solvent, which was purified by column chromatography on silica gel with petroleum ether (60-90 °C) and CH_2Cl_2 (1:1, *v/v*) as eluent. The final product was dissolved in a small amount of hot $CHCl_3$ (~10 mL) and then CH_3OH (~30 mL) was added as antisolvent. The mixture was cooled to room temperature, and final product was collected by filtration and then washed with CH_3OH for three times (10 mL × 3). Compound **DPP-1/4** was obtained as a dark red solid (71mg) in 62% yield. ^{1}H NMR ($CDCl_3$, 400 MHz): δ 9.00 (m, 2H), 7.59 (m, 4H), 7.43 (d, J = 4.0 Hz, 2H), 7.29 (d, J = 8.0 Hz, 4H), 4.08 – 3.97 (m, 4H), 2.53 (s, 6H), 1.99 (m, 2H), 1.52 – 1.50 (m, 2H), 1.30 – 1.23 (m, 2H), 0.97 – 0.92 (m, 12H). ^{13}C NMR (*o*-$C_6D_4Cl_2$, 125 MHz, 100 °C): δ 161.3, 148.9, 140.1, 139.2, 136.3, 130.9, 130.1, 127.1, 126.1, 123.8, 108.6, 47.5, 35.4, 27.1, 16.5, 15.3, 10.7. HRMS (MALDI-TOF) m/z: calcd. for $C_{38}H_{40}N_2O_2S_4$, 684.1973; found, 684.1973. Anal. calcd. for $C_{38}H_{40}N_2O_2S_4$•$(H_2O)_{0.2}$: C, 66.28; H, 5.91; N, 4.07; S, 18.62; Found: C, 66.04; H, 5.83; N, 4.11; S, 18.57.

Synthesis of **DPP-2/6**

To a Schlenk flask equipped with a stir bar was added compound **M3** (69 mg, 0.41 mmol), compound **M4** (100 mg, 0.15 mmol), $Pd(PPh_3)_4$ (9 mg, 7.8 μmol). The vessel was sealed and evacuated/backfilled with nitrogen for three times, followed by the addition of toluene (20 mL) and a degassed 2.0 mL of saturated aqueous solution of $NaHCO_3$ via syringe. The mixture was heated at 90 °C for 8 h. After cooling, the mixture was directly evaporated to remove the solvent, which was purified by column chromatography on silica gel with petroleum ether (60-90 °C) and CH_2Cl_2 (2:1, *v/v*) as eluent. The final product was dissolved in a small amount of hot $CHCl_3$ (~8 mL) and then CH_3OH (~30 mL) was added as antisolvent. The mixture was cooled to room temperature, and final product was collected by filtration and then washed with CH_3OH for three times (10 mL × 3). Compound **DPP-2/6** was obtained as a dark red solid (78 mg) in 69% yield. ^{1}H NMR ($CDCl_3$, 400 MHz): δ 8.94 (m, 2H), 7.67-7.50 (m, br, 4H), 7.42 (d, 2H, J = 3.6 Hz), 7.28 (d, 4H, J = 8.1 Hz), 4.08 (d, 4H, J = 6.8 Hz), 2.53 (s, 6H), 1.94-1.93 (m, 2H), 1.42-1.28 (m, 16H), 0.93-0.85 (m, 12H). ^{13}C NMR ($CDCl_3$, 125 MHz): δ 161.7, 149.2, 139.9, 139.7,

136.9, 129.9, 128.5, 126.6, 126.4, 124.1, 108.2, 46.0, 39.3, 30.4, 30.4, 28.6, 23.7, 23.1, 15.5, 14.1, 10.6. HRMS (MALDI-TOF) m/z: calcd. for $C_{44}H_{52}N_2O_2S_4$, 768.2912; found, 768.2909. Anal. calcd. for $C_{44}H_{52}N_2O_2S_4$: C, 68.71; H, 6.81; N, 3.64; S, 16.67; Found: C, 68.66; H, 6.83; N, 3.49; S, 16.64.

Synthesis of **DPP-8/12**

To a Schlenk flask equipped with a stir bar was added compound **M3** (46 mg, 0.275 mmol), compound **M5** (100 mg, 98 μmol), $Pd(PPh_3)_4$ (5.7 mg, 4.9 μmol). The vessel was sealed and evacuated/backfilled with nitrogen for three times, followed by the addition of toluene (20 mL) and a degassed 2.0 mL of saturated aqueous solution of $NaHCO_3$ via syringe. The mixture was heated at 90 °C for 8 h. After cooling, the mixture was directly evaporated to remove the solvent, which was purified by column chromatography on silica gel with petroleum ether (60-90 °C) and CH_2Cl_2 (1:1, *v/v*) as eluent. The final product was dissolved in a small amount of $CHCl_3$ (~5 mL) and then CH_3OH (~30 mL) was added as antisolvent. The mixture was cooled to room temperature, and final product was collected by filtration and then washed with CH_3OH for three times (10 mL × 3). Compound **DPP-8/12** was obtained as a dark red solid (82 mg) in 76% yield. ^{1}H NMR ($CDCl_3$, 400 MHz): δ 8.93 (m, 2H), 7.58 (d, *J* = 8.0 Hz, 4H), 7.42 (d, *J* = 4.0 Hz, 2H), 7.28 (m, 4H), 4.06 (d, *J* = 8.0 Hz, 4H), 2.53 (s, 6H), 1.993 – 1.96 (m, 2H), 1.33 – 1.21 (m, 64H), 0.87 – 0.82 (m, 12H). ^{13}C NMR ($CDCl_3$, 100 MHz): δ 161.7, 149.2, 139.9, 139.8, 136.8, 129.9, 128.5, 126.7, 126.4, 124.0, 108.2, 46.3, 37.9, 31.9, 31.9, 31.4, 30.1, 29.7, 29.7, 29.6, 29.4, 29.3, 26.4, 22.7, 22.7, 15.5, 14.1. HRMS (MALDI-TOF) m/z: calcd. for $C_{68}H_{100}N_2O_2S_4$, 1104.6668; found, 1104.6658. Anal. calcd. for $C_{68}H_{100}N_2O_2S_4 \bullet (H_2O)_{0.4}$: C, 73.38; H, 9.13; N, 2.52; S, 11.52; Found: C, 73.19; H, 9.06; N, 2.54; S, 11.67.

2. Single-molecule conductance measurement and data analysis

As shown in Figure S1, a homemade STM-BJ setup was used to perform single-molecule conductance measurements. The silicon wafer (treat with piranha solution before use) with the surface evaporated with 200 nm gold was installed on the pedestal as the substrate. The other electrode, a piece of gold wire (0.25 mm in diameter) with the tip burned into a ball by butane flame, is fixed on the top of the substrate. The tip and the substrate are respectively connected with external circuits to monitor the current through them in real-time. A shield box and optical shockproof platform were used to shield electromagnetic and mechanical interference. The experiment was carried out under ambient conditions.

Nonpolar 1,3,5-Trimethylbenzene (TMB) was used to prepare the solution containing 0.1mmol/L target molecule to reduce the leakage current. Before the experiment, the tip should be close to the substrate but not contacted. Then a drop of the solution was dropped on the

substrate and submerged the tip. The piezo and stepping motor work together to control the tip contact and leave the substrate. When two electrodes break to form a gap matching the molecular size, the target molecule would be connected to the electrode through the anchoring groups at both ends. In this way, the conductance of the single-molecule junction was measured. During the repeated break/re-connecting process, for statistical analysis, one thousand current-time curves for each test were recorded and converted into conductance-distance curves. The construction of 1D and 2D conductance diagrams and more detailed data analysis methods can refer to our previous work.[S4-S6]

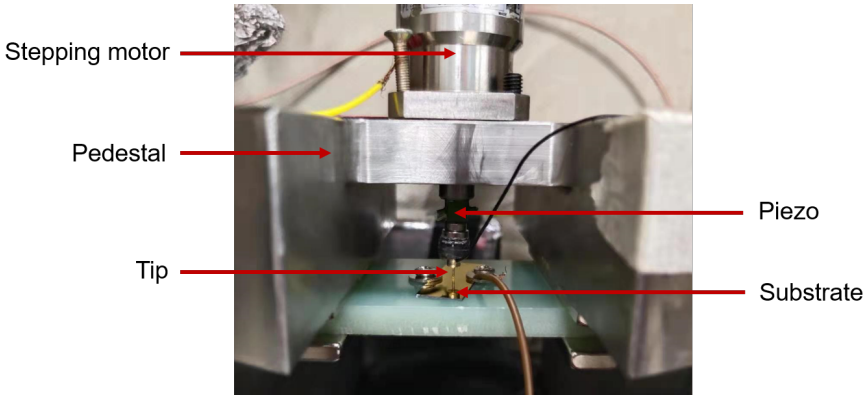

Figure S1. The photo of the STM-BJ setup.

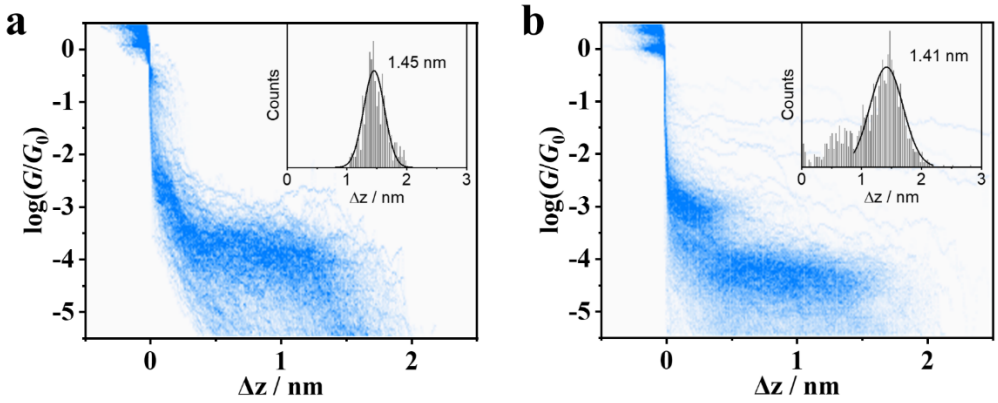

Figure S2. 2D conductance histogram of a) **DPP-2/6**, b) **DPP-8/12**. The inset is the relative displacement distribution.

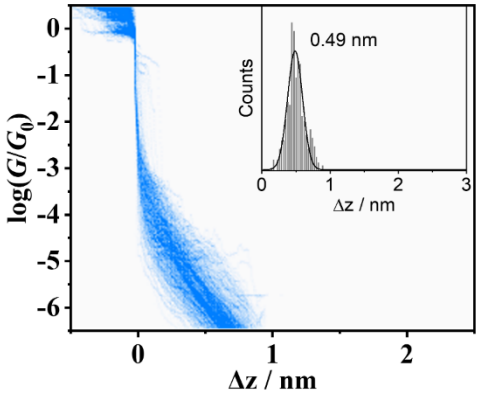

Figure S3. 2D conductance histogram of blank experiment. The inset is the relative displacement distribution.

3. Theoretical calculations

3.1 DFT calculation

The optimized geometry and ground state Hamiltonian and overlap matrix elements of each structure was self-consistently obtained using the SIESTA[S7] implementation of density functional theory (DFT). SIESTA employs norm-conserving pseudo-potentials to account for the core electrons and linear combinations of atomic orbitals to construct the valence states. The generalized gradient approximation (GGA) of the exchange and correlation functional is used with the Perdew-Burke-Ernzerhof parameterization (PBE)[S8] a double-ζ polarized (DZP) basis set, a real-space grid defined with an equivalent energy cut-off of 200 Ry. The geometry optimization for each structure is performed to the forces smaller than 10 meV/Ang. We know the solvent effect would be an important factor which could induce the geometrical changes of the backbone in realistic single-molecule conductance measurements. However, considering the heavy computational expenses, we carried out the investigation in the energetics and the effect of series of manual torsion angles in the backbone for the gas-phase molecules.[S9]

3.2 Transport calculations

The mean-field Hamiltonian obtained from the converged DFT calculation or a tight-binding Hamiltonian (using single orbital energy site per atom with Hückel parameterisation) was combined with our home-made implementation of the non-equilibrium Green's function method, GOLLUM[S10] to calculate the phase-coherent, elastic scattering properties of the each system consisting of left gold (source) and right gold (drain) leads and the scattering region (molecule **DPP**, **DPP-1/4**, **DPP-2/6**, **DPP-8** and **DPP-8/12**). The transmission coefficient $T(E)$ for electrons of energy E (passing from the source to the drain) is calculated via the relation:

$$T(E) = Trace\left(\Gamma_R(E)G^R(E)\Gamma_L(E)G^{R\dagger}(E)\right)$$

In this expression, $\Gamma_{L,R}(E) = i\left(\Sigma_{L,R}(E) - \Sigma_{L,R}{}^{\dagger}(E)\right)$ describe the level broadening due to the coupling between left (L) and right (R) electrodes and the central scattering region, $\Sigma_{L,R}(E)$ are the retarded self-energies associated with this coupling and $G^R(E) = (ES - H - \Sigma_L - \Sigma_R)^{-1}$ is the retarded Green's function, where H is the Hamiltonian and S is overlap matrix. Using obtained transmission coefficient $T(E)$, the conductance could be calculated by Landauer formula ($G = G_0 \int dE\, T(E)(-\partial f/\partial E)$) where $G_0 = 2e^2/h$ is conductance quantum. $f(E) = (1 + exp((E - E_F)/k_BT))^{-1}$ is the Fermi–Dirac distribution function, T is the temperature,

and k_B = 8.6 × 10^{-5} eV/K is Boltzmann's constant. Transmission coefficients are the conductance in zero-temperature approximation.

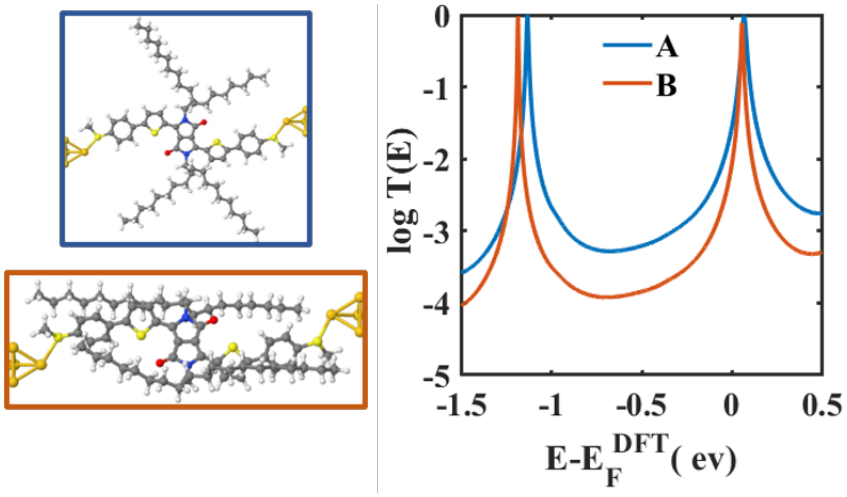

Figure S4. DFT-based transmission functions for *A* and *B* conformers of **DPP-8/12**. Corresponding transmission coefficients against energy relative to the Fermi energy E_F predicted by DFT.

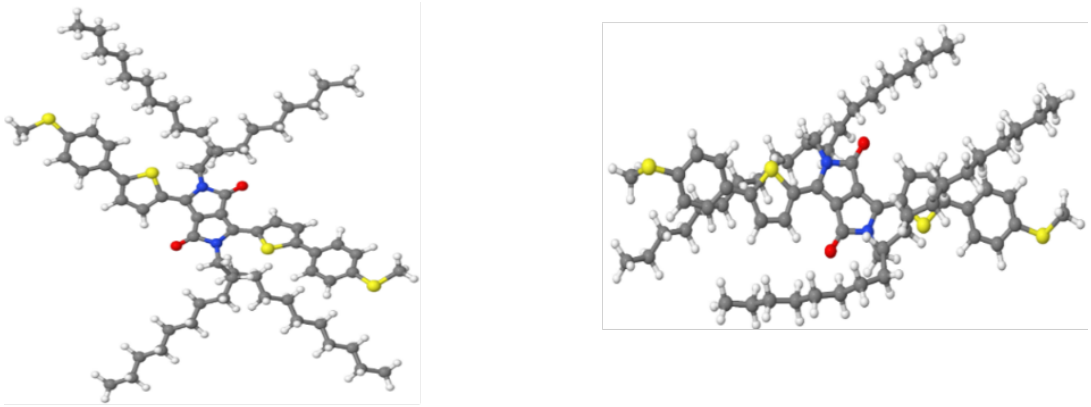

Figure S5. Conformations of **DPP-8/12** in terms of different positions alkyl side chains relative to the DPP core where *A*' is sticking out into space with the left side of dihedral angle between the thophene and DPP-core is 8° and the right side is 8.9°, *B*' is stacked with the DPP-backbone of the molecule space and more energetically stable compared to conformer *A'* by 0.55 eV with the left side of dihedral angle between the thophene and DPP-core is 19.7° and the right side is 12.1°.

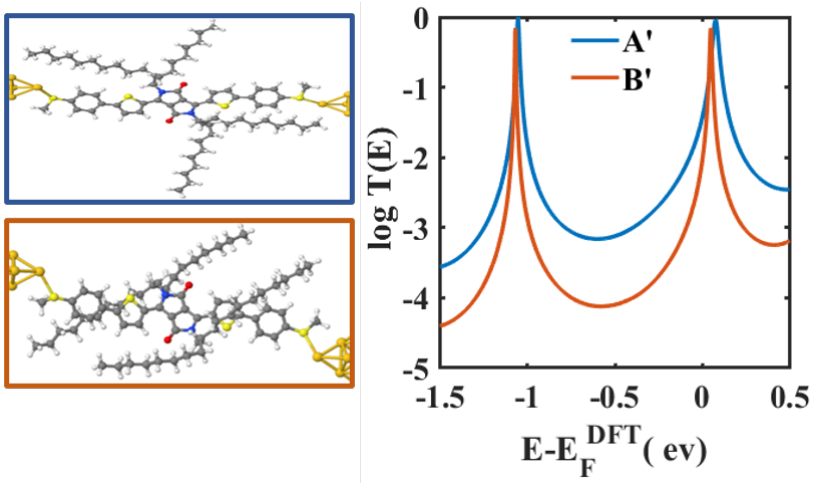

Figure S6. DFT-based transmission functions for *A*' and *B*' conformers of **DPP-8/12**. Corresponding transmission coefficients against energy relative to the Fermi energy E_F predicted by DFT.

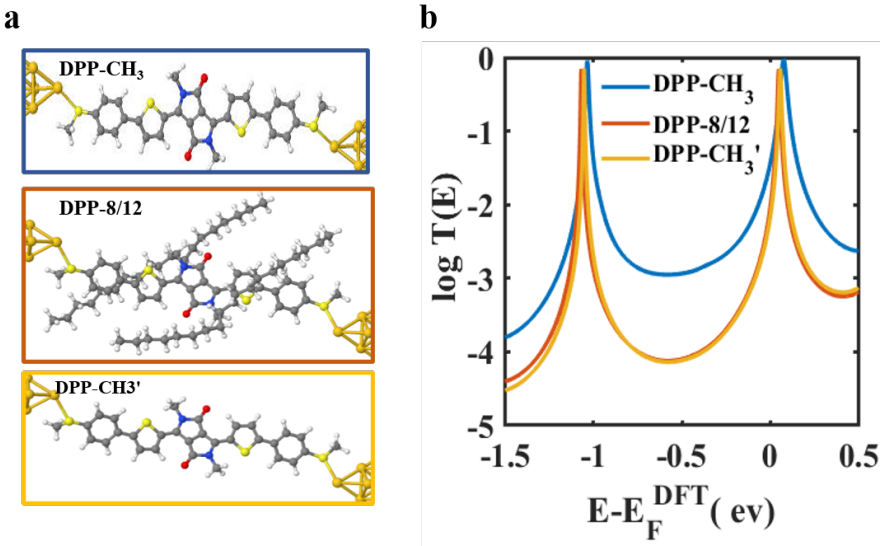

Figure S7. a) Models of single-molecule junctions with DPP molecules (O-H) in different geometrical changes, (Top panel: rather planar **DPP-CH₃** molecule after geometrical optimization. And Middle panel: molecule with a twisted backbone induced by the alkyl side chains (**DPP-8/12**), Bottom panel: molecule **DPP-CH₃'** with replaced methyl group for the long alkyl chains and the backbone unchanged based on the structure in Middle panel. b) Transmission spectra in units of quantum conductance G_0 =77 μs against Fermi energy E_F relative to the predicted value E_F^{DFT} by DFT.

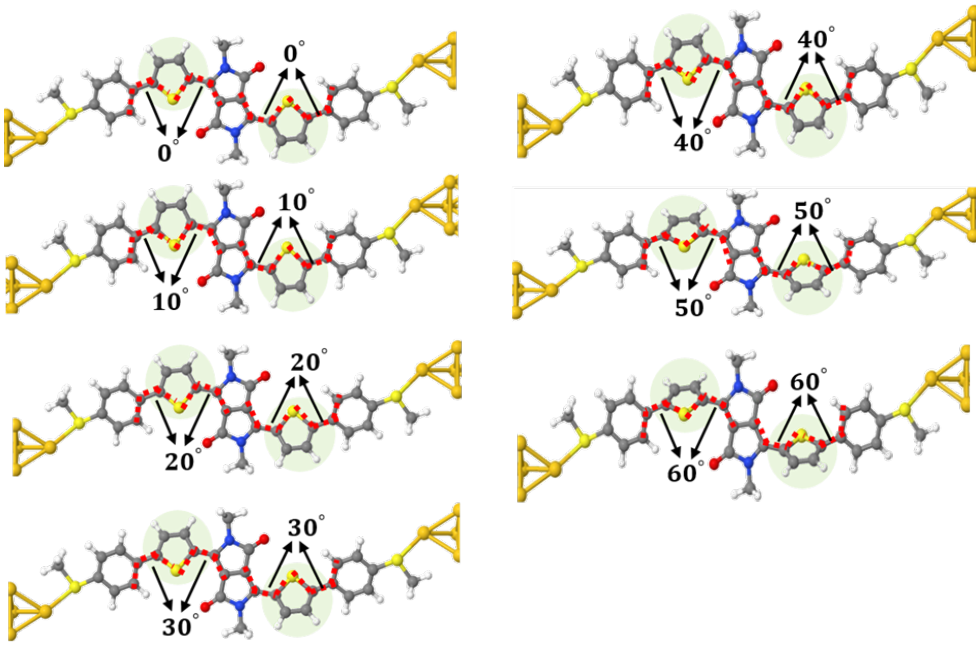

Figure S8. Models of single-molecule junctions with various thiophene-ring rotation (indicated by the green shaded regions) angles relative to the rest part of the whole molecule from 10^o to 60^o(indicated by the dashed red line).

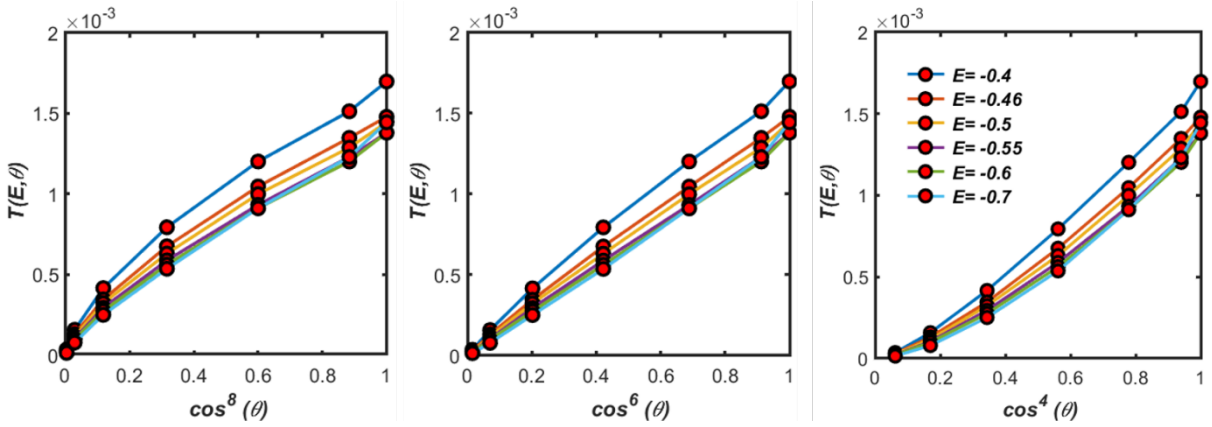

Figure S9. Transmission functions of molecular junctions with various thiophene-ring rotation angles θ (shown in Figure S8) against $\cos^8\theta$ and $\cos^4\theta$ at energy points around the middle of HOMO-LUMO gap, e.g. -0.4, -0.46, -0.5, -0.55, -0.6, -0.7. E is the energy relative to the Fermi energy predicted by DFT. θ is the dihedral angle of the flanking thiophenes relative to the rest part of the whole molecule (indicated by the dashed red lines in Figure S8).

4. NMR spectra

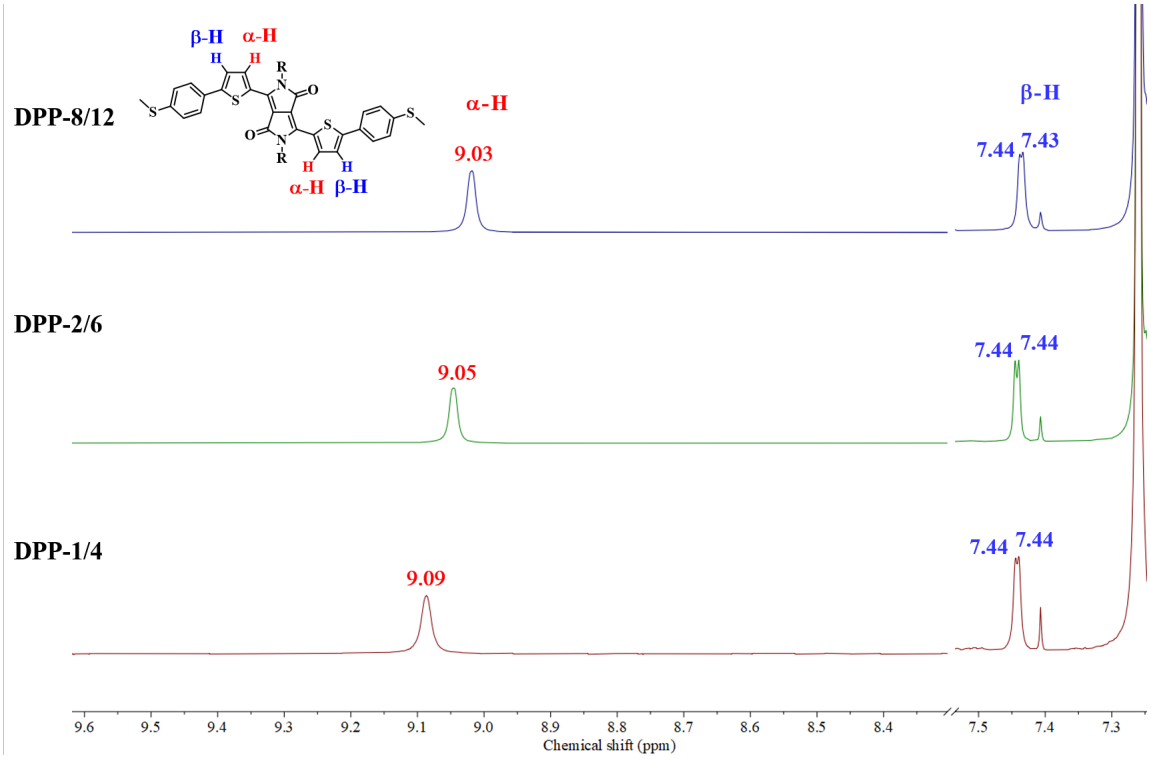

Figure S10. ^{1}H NMR spectra (400 MHz, 233 K) for **DPP-1/4**, **DPP-2/6**, and **DPP-8/12** in $CDCl_3$; the concentration of each sample was 5×10^{-4} M.

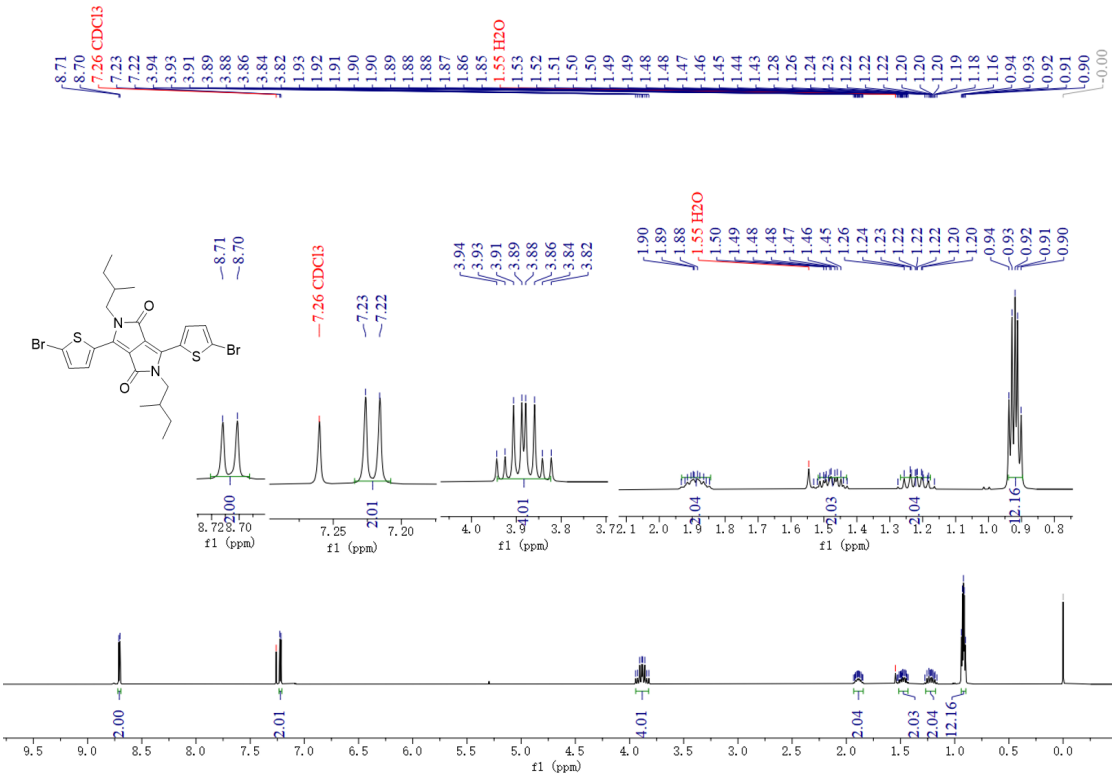

Figure S11. ^{1}H NMR spectrum of **M2** in $CDCl_3$.

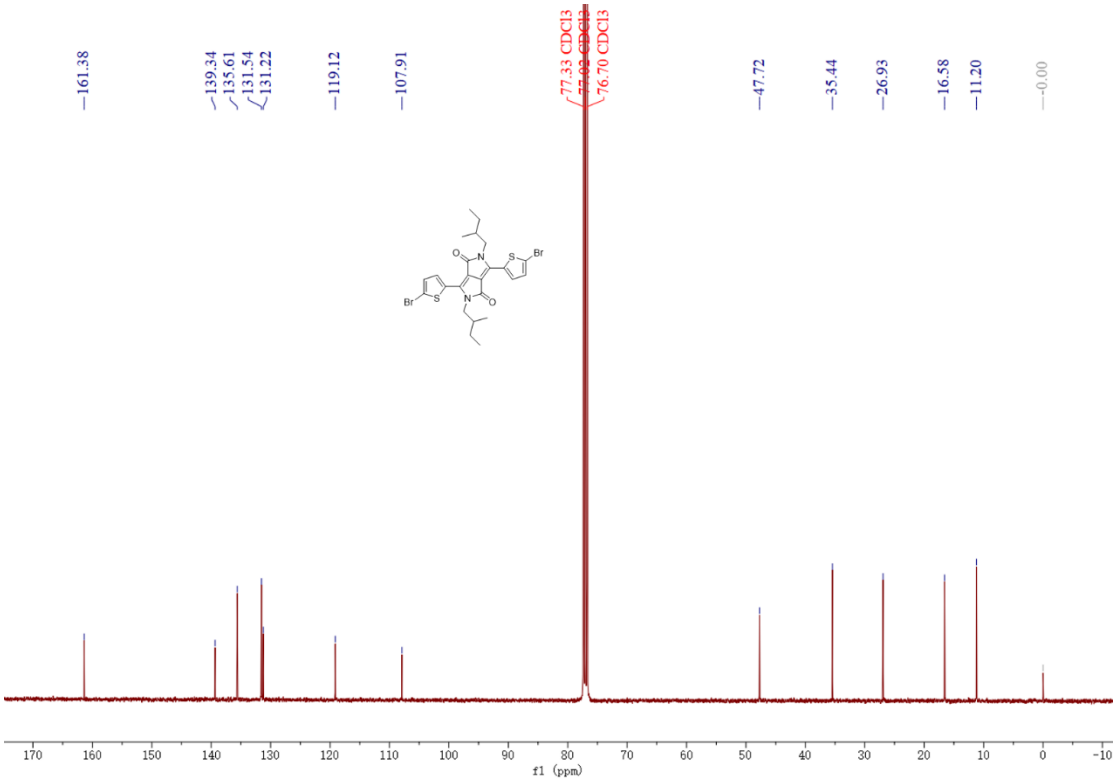

Figure S12. ^{13}C NMR spectrum of **M2** in $CDCl_3$.

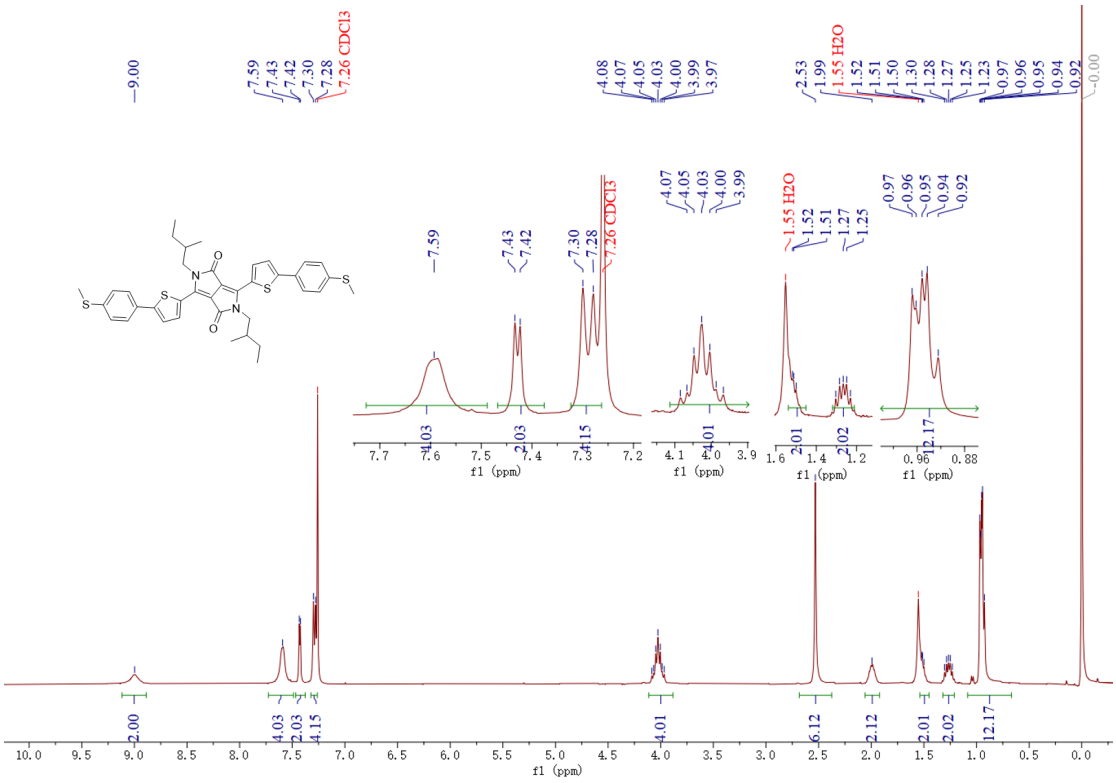

Figure S13. ^{1}H NMR spectrum of **DPP-1/4** in $CDCl_3$.

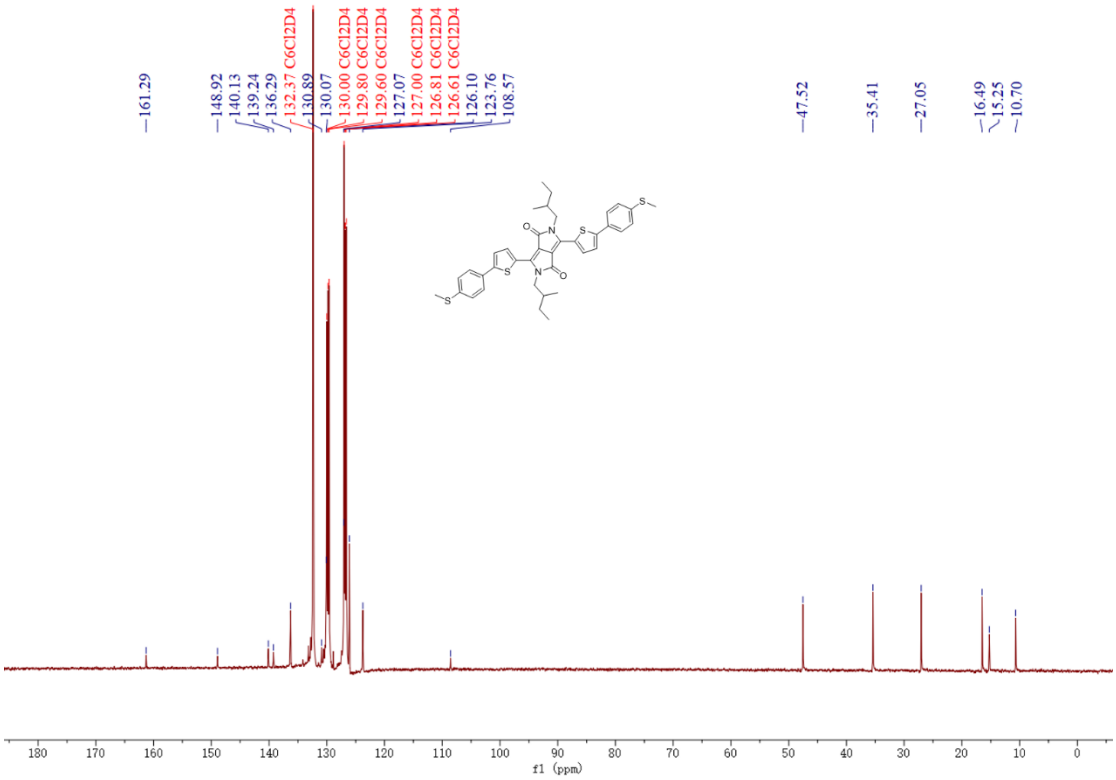

Figure S14. ^{13}C NMR spectrum of **DPP-1/4** in *o*-$C_6D_4Cl_2$.

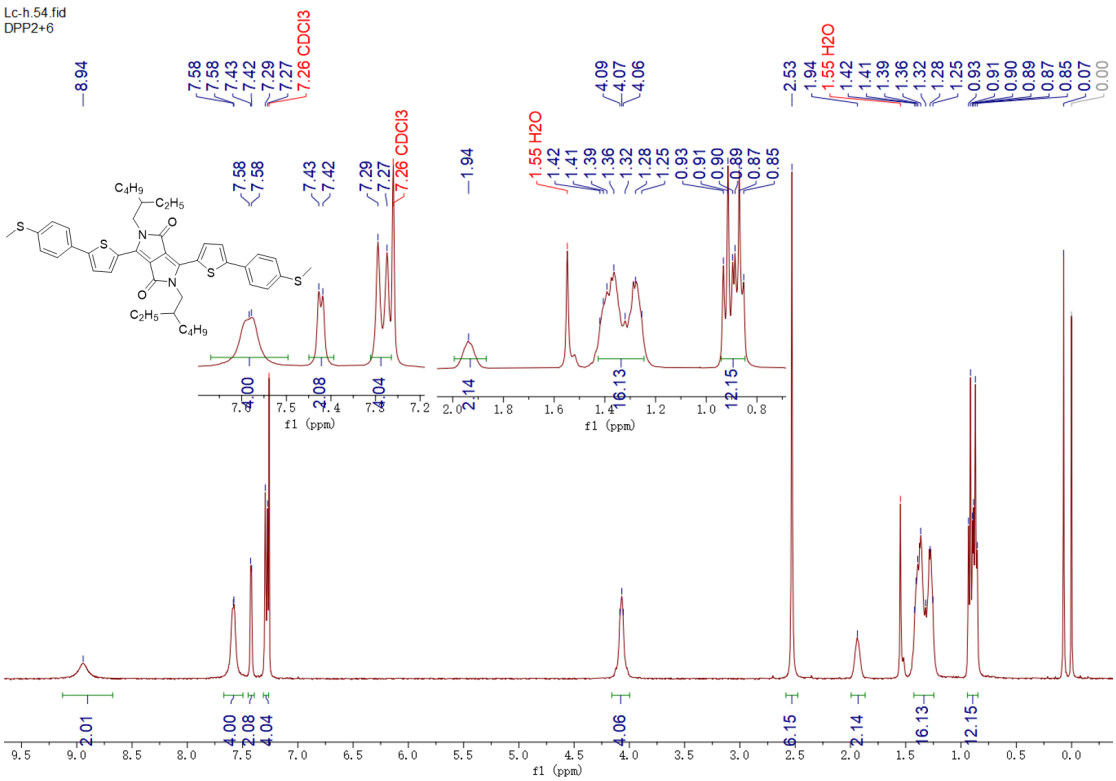

Figure S15. ^{1}H NMR spectrum of **DPP-2/6** in $CDCl_3$.

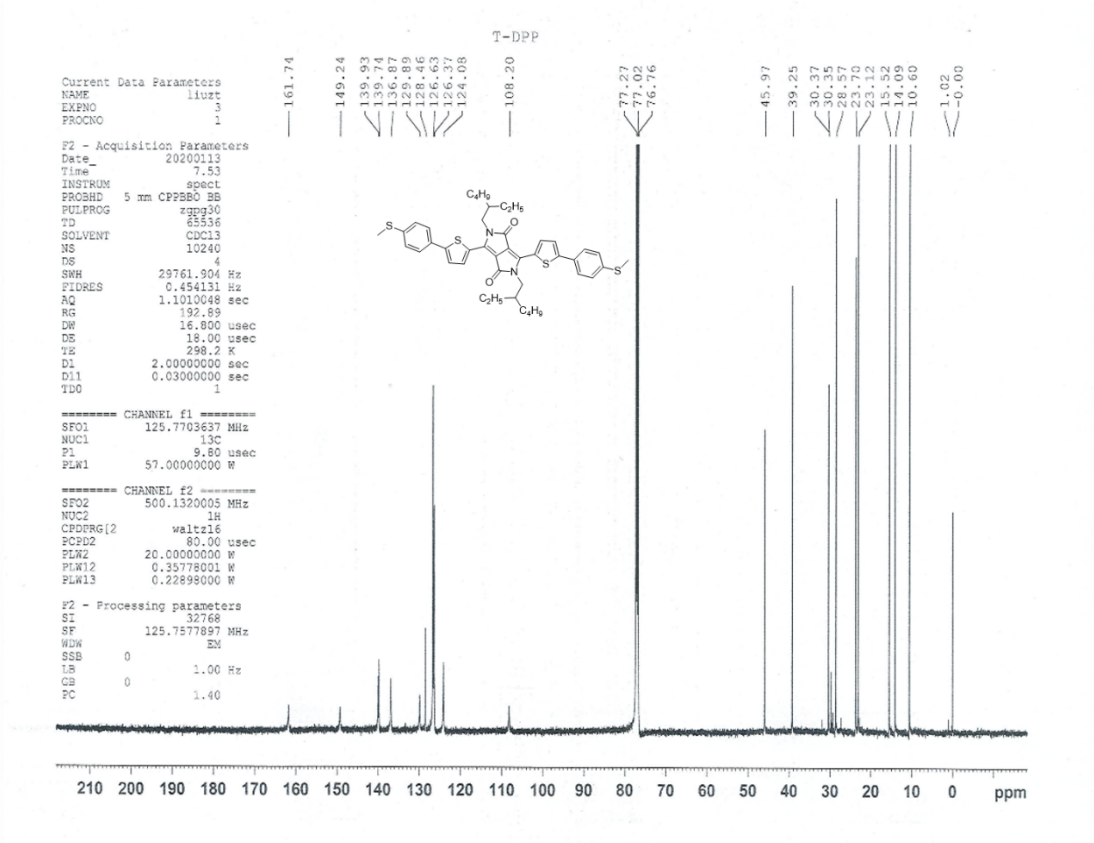

Figure S16. ^{13}C NMR spectrum of **DPP-2/6** in $CDCl_3$.

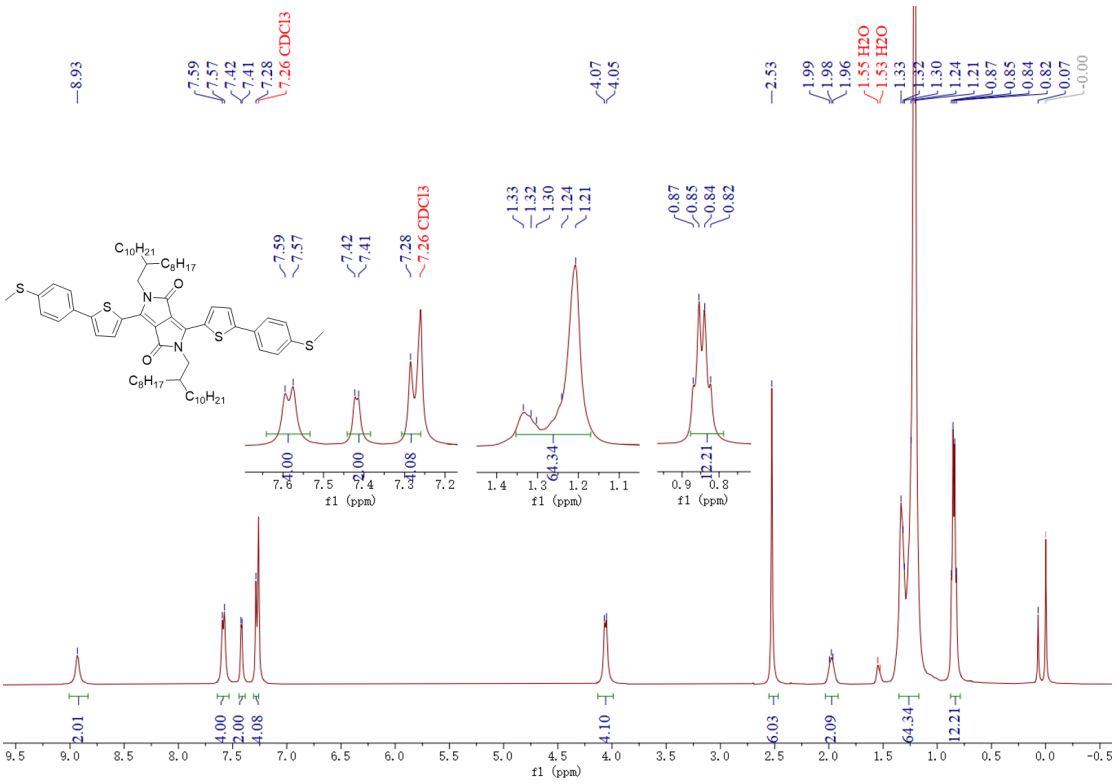

Figure S17. ^{1}H NMR spectrum of **DPP-8/12** in $CDCl_3$.

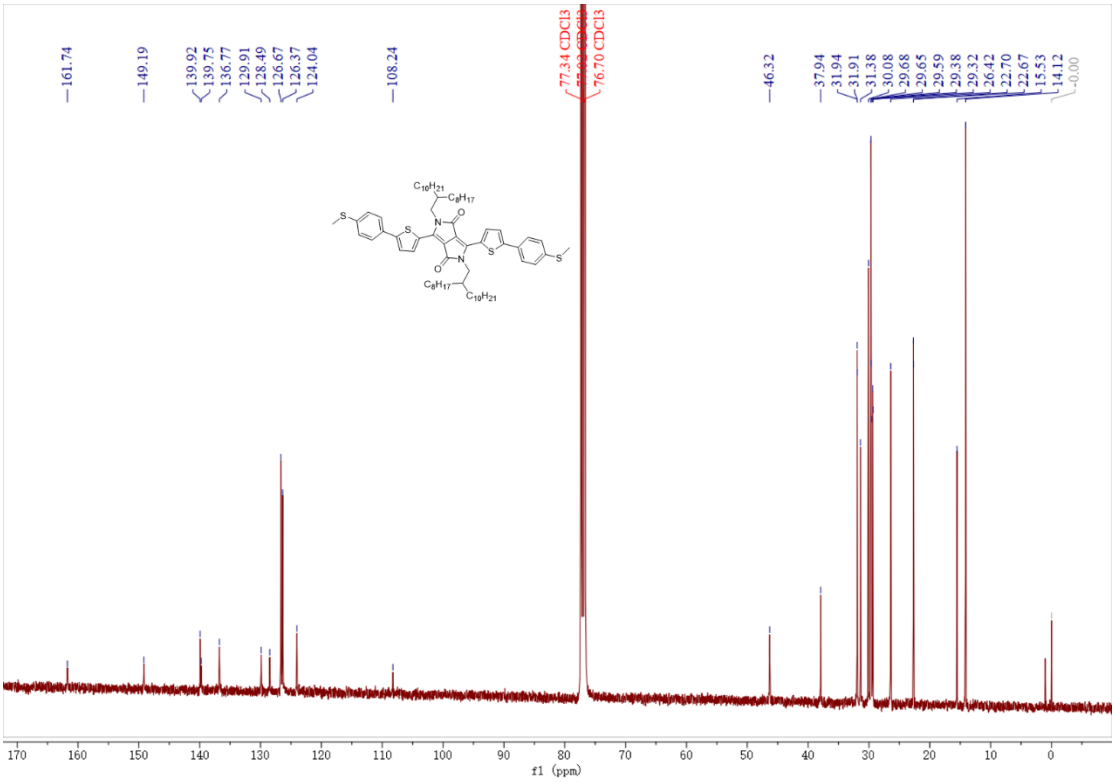

Figure S18. ^{13}C NMR spectrum of **DPP-8/12** in $CDCl_3$.

5. References

[S1] Mueller, C. J.; Singh, C. R.; Fried, M.; Huettner, S.; Thelakkat, M. *Adv. Funct. Mater.* **2015**, *25*, 3454-3454.

[S2] Sonar, P.; Zhuo, J. M.; Zhao, L. H.; Lim, K. M.; Chen, J. H.; Rondinone, A. J.; Singh, S. P.; Chua, L. L.; Ho, P. K. H.; Dodabalapur, A. *J. Mater. Chem.* **2012**, *22*, 17284-17292.

[S3] Carsten, B.; Szarko, J. M.; Lu, L.; Son, H. J.; He, F.; Botros, Y. Y.; Chen, L. X.; Yu, L. *Macromolecules* **2012**, *45*, 6390-6395.

[S4] Tan, Z.; Zhang, D.; Tian, H. R.; Wu, Q.; Hou, S.; Pi, J.; Sadeghi, H.; Tang, Z.; Yang, Y.; Liu, J.; Tan, Y. Z.; Chen, Z. B.; Shi, J.; Xiao, Z.; Lambert, C.; Xie, S. Y.; Hong, W. *Nat. Commun.* **2019**, *10*, 1748.

[S5] Bai, J.; Daaoub, A.; Sangtarash, S.; Li, X.; Tang, Y.; Zou, Q.; Sadeghi, H.; Liu, S.; Huang, X.; Tan, Z.; Liu, J.; Yang, Y.; Shi, J.; Meszaros, G.; Chen, W.; Lambert, C.; Hong, W. *Nat. Mater.* **2019**, *18*, 364-369.

[S6] Liu, J.; Zhao, X.; Zheng, J.; Huang, X.; Tang, Y.; Wang, F.; Li, R.; Pi, J.; Huang, C.; Wang, L.; Yang, Y.; Shi, J.; Mao, B.-W.; Tian, Z.-Q.; Bryce, M. R.; Hong, W. *Chem* **2019**, *5*, 390-401.

[S7] Soler, J. M.; Artacho, E.; Gale, J. D.; García, A.; Junquera, J.; Ordejón, P.; Sánchez-Porta, D. *J. Phys. Condens. Matter.* **2002**, *14*, 2745-2779.

[S8] Perdew, J.; Burke, P. K.; Ernzerhof, M. *Phys. Rev. Lett.* **1998**, *80*, 891.

[S9] Tang, Z.; Hou, S.; Wu, Q.; Tan, Z.; Zheng, J.; Li, R.; Liu, J.; Yang, Y.; Sadeghi, H.; Shi, J.; Grace, I.; Lambert, C. J.; Hong, W. *Sci. Bull.* **2020**, *65*, 944-950.

[S10] Ferrer, J.; Lambert, C. J.; García-Suárez, V. M.; Manrique, D.; Visontai, D.; Oroszlany, L.; Rodríguez-Ferradás, R.; Grace, I.; Bailey, S. W. D.; Gillemot, K.; Sadeghi, H.; Algharagholy, L. A., *New J. Phys.* **2014**, *16*, 093029.